Journal of Applied Polymer Science

Controlled-release drug carriers based hierarchical silica microtubes templated from cellulose acetate nanofibers

Chengying Jia,[1,2] Junlong Song,[1,3] Yongcan Jin,[1] Orlando J. Rojas[3]

[1]Jiangsu Provincial Key Lab of Pulp and Paper Science and Technology, Nanjing Forestry University, Nanjing 210037, China
[2]Quzhou Branch of China National Pulp and Paper Research Institute, Quzhou, Zhejiang 324022, China
[3]Department of Forest Products Technology, Faculty of Chemistry and Materials Sciences, Aalto University, Aalto FI 00076, Finland
Correspondence to: J. Song (E-mail: junlong.song@njfu.edu.cn)

ABSTRACT: We report a facile method to synthesize hollow silica microtubes (SMTs) from electrospun cellulose acetate fiber precursors. Specific surface areas of up to 765 m^2/g (Brunauer–Emmett–Teller) were measured for the SMTs, which had a typical wall thickness of ~100 nm and submicron inner diameters. An average pore size of 4.6 nm and pore volume of 0.41 cm^3/g were derived from Barrett–Joyner–Halenda fitting, whereas Horvath–Kawazoe pore size distribution analysis revealed microporous median pore size and maximum pore volume of 0.7 nm and 0.18 cm^3/g, respectively. The as-prepared SMTs featuring micro- and mesoporous structures in the walls where amino-functionalized to facilitate a very high drug loading (15% by weight). Drug release profile revealed sustained release rates (79% of acetylsalicylic acid was released after 6 h). It is concluded that the high drug loading and sustained release resulted from the advantageous integration of SMTs' hollow structure and wall mesoporosity. © 2015 Wiley Periodicals, Inc. J. Appl. Polym. Sci. **2015**, *132*, 42562.

KEYWORDS: applications; cellulose and other wood products; drug delivery systems; electrospinning; porous materials

Received 9 April 2015; accepted 31 May 2015
DOI: 10.1002/app.42562

INTRODUCTION

Hollow-structured mesoporous materials (HMMs) have recently attracted considerable attention because of a combination of advantages from their hollow architecture and mesoporous structure. Owing to their low density, large void space, and specific surface area, HMMs are promising in various applications, such as adsorption and storage, confined catalysis, optical devices, enzyme immobilization, etc.[1–5] In addition to such possibilities, the excellent biocompatibility, biodegradability, and facile surface modification of silica-based HMMs make them particularly suitable for drug release control and targeted delivery as well as simultaneous diagnosis and therapy of cancers.[4,6–17]

A template-directed synthesis strategy is an ideal tool to fabricate hollow materials because the resultant physical dimensions can be precisely controlled and monodisperse samples can be harvested in large quantity. In general, there are two main synthetic routes to produce HMMs, soft- and hard-templating.[18–21] For example, an amphiphilic block copolymer[22] and a mixture of aqueous ammonia and tartaric acid[23] were used for soft-templating hollow mesoporous silica nanoparticles with tunable shell thickness and pore size and phosphorylated silica nanotubes with high length-to-diameter ratios, respectively. Silicate hollow nanotubes were synthesized via hard-templating by replicating carbon nanotubes via a sol–gel process with heat treatment.[10]

Electrospinning is a simple and efficient process to produce nanofibers,[21,24–28] which can be used directly or acted as templates for creating new functional nanoproducts or manipulating molecular self-assembly.[29] For instance, hollow TiO_2 fibers were obtained from electrospun poly(ethylene oxide)[30] or polyacrylonitrile (PAN) fibers.[31] Conductive polyaniline nanotubes were prepared from poly(vinyl alcohol).[32] ZnO hollow nanofibers were templated from electrospun fibers of PAN and polyvinylpyrrolidone,[33] polycarbonate,[34] polyvinyl-acetate,[35] and PAN.[36] Macroporous poly(3,4-ethylenedioxythiophene)/poly (4-styrene sulfonate) films with empty channels were fabricated by using electrospun polyvinylpyrrolidone/poly(methyl methacrylate) nanofiber as a sacrificial template.[37] Submicron silver tubes were prepared from electrospun polycarbonate fiber templates,[38] and porous nanofiber mats of poly(3,4-ethylenedioxythiophene) with electrical conductivity was grown on electrospun polystyrene fiber templates.[39] Long and uniform Al_2O_3 microtubes were fabricated by atomic layer deposition on electrospun PVA microfiber templates.[40] Huang *et al.*[41]

developed a method to produce silica hollow fibers by surface-initiated atom transfer radical polymerization from poly(methyl methacrylate-*co*-vinylbenzyl chloride) electrospun fibers combined with sol–gel process and subsequent calcination.

Cellulose acetate (CA) has good filament-forming property[42] and has abundant OH groups in its molecules, which makes its electrospun nanofibers ideal templates for tubular nanofabrication.[43,44] One example is that it can interact with tetraethoxysilane (TEOS), or can form hydrogen bonds with silica,[45–47] for the formation of silica microtubes (SMTs). Electrospun CA nanofibers can be ideal templating matrices to fabricate tubular materials. CA is easy to dissolve in common solvents and easy to electrospin. In this work, we present a new strategy to synthesize SMTs from electrospun CA fiber templates combined with a sol–gel reaction with TEOS in alkaline conditions and subsequent calcination. The obtained system was loaded with acetylsalicylic acid (ASA), a classical drug with pharmacological functions (antipyretic, analgesic, anti-inflammatory, antirheumatism, antiplatelet aggregation, etc.).[48,49] Demonstration of controlled release is provided as an approach to reduce the adverse effects of ASA when used in large doses and for prolonged time, including gastrointestinal system irritation, ulcer, or hemorrhage. What is more, this facile method of advanced silica-based materials synthesis fits to sustainable engineering and green chemistry concept as well.[47,50]

EXPERIMENTAL

Materials

CA (54.5–56 wt % acetyl content) was provided by Sinopharm Chemical Regent Co. (Shanghai, China). ASA (99%) and 3-amino propyltriethoxy silane (APTES, 99%) were supplied by Aladdin (Shanghai, China). Toluene, acetone, TEOS, cetyltrimethyl ammonium bromide (CTAB), aqueous ammonia (25 wt %), and ethanol (>99.7%) were purchased from Everbright Chemical (Nanjing, China). All chemicals were used as received, without further purification. Solutions were prepared using distilled/deionized water, which was treated with a Milli-Q system (Millipore Corp., Billerica, MA).

Preparation of CA Electrospun Fibers

CA fibers were produced following our earlier report.[21] Briefly, a solution of CA in acetone and water (90 : 10 v/v) at 13 wt % concentration was loaded in a syringe equipped with a metallic needle gauge 22 (ID = 1.2 mm) with a flattened tip. An aluminum foil was used as collector of the fibers electrospun by using a field strength of 20 kV/15 cm at a polymer solution feed rate of 3 mL/h.

Silica Microtubes

The SMTs were prepared using CA electrospun fibers as the template. CTAB was used to couple CA fiber surfaces with the silica sol and the generator of micro- and mesopores. Water and ethanol were used as solvent, aqueous ammonia as the catalyst, and TEOS as the source of silica. Initially, 20 mg of CA electrospun fibers, 27 mg CTAB, and 0.4 mL of aqueous ammonia were combined in a solution containing water (45 mL) and ethanol (15 mL). The system was dispersed by ultrasonication for 30 min followed by slow addition of 160 μL TEOS dispersed in 3.2 mL ethanol. After reaction at 30°C ±1°C for 2–3 h, the hybrid silica/CA electrospun fibers were washed with ethanol to remove unreacted regents, and then dried at room temperature. The final SMTs were obtained after calcination to remove the organic (CA) template by using a muffle operated at 600°C for 6 h.

Functionalization of SMTs

Silica-based nanomaterials carrying surface Si—OH groups are conveniently modified with silanes[51] and were used here as a switchable platform for selective loading of molecules, depending on the surface charge characteristics.[10] In this work, the modification was carried out by postgrafting of SMT with APTES: 0.2 g SMTs and APTES (5 mL) were placed in a flask filled with 50 mL toluene. After ultrasonication, the dispersion was refluxed at 120°C for 6 h and then subjected to centrifugation, sequential washing with toluene (×2) and ethanol (×3) and drying in an oven at 105°C. The obtained, functionalized SMT is thereafter referred as FSMT.

Acetylsalicylic Acid Loading and Release

In this work, ASA was chosen as a model drug because of its small molecular size, good pharmacological activity, and short biological half-life.[48,49] FSMTs (0.15 g) were added into 18 mL ASA solution in anhydrous ethanol at a concentration of 20 mg mL^{-1}. The mixture was stirred for 24 h with a magnetic stirrer at room temperature, then centrifuged to collect the sample incorporating ASA, and washed with anhydrous ethanol to remove excess drug present on the surface. The FSMT loaded with ASA (FSMT-ASA) was dried in a vacuum oven at 40°C. The amount of drug loading was calculated using a thermogravimetric analyzer. 0.12 g FSMT loaded with ASA was placed in an Erlenmeyer flask with 120 mL of phosphate buffer solution of pH = 7.4 and shaken at 37°C at 200 rpm. At given time intervals, 3.6 mL suspension were withdrawn and centrifuged to remove the solid. The solution was characterized by UV-vis absorbance at 296 nm to quantify the amount of drug released.[48,49]

Physical and Chemical Characterizations

Scanning electron microscopy (SEM) images of electrospun fibers and SMT samples sputter-coated with platinum were obtained with a JEOL thermal field-emission scanning electron microscope (JSM-7600F) to determine the morphology and size of the samples. Transmission electron microscopy (TEM) images of SMT were obtained by a JEOL JEM-1400 electron microscope. Samples of SMTs were fractured into a powder by using tweezers prior to TEM measurements. The powder was then dispersed in absolute ethanol with ultrasonication for 10 min and then dropped onto copper grids with carbon films.[18] Fourier transform infrared (FTIR) spectra of SMT, FSMT, and FSMT-ASA were acquired with a Bruker VERTEX80 spectrometer. Approximately, 1 mg of the sample and 200 mg of KBr were mixed and pressed into disks for sample preparation. Small-angle X-ray diffraction (SAXD) patterns of SMT were recorded on an Ultima IV (Rigaku Corp., Japan) with CuKα radiation. N_2 adsorption and desorption isotherms of SMT were performed using a Micromeritics ASAP 2020 instrument. The specific surface area was determined by the Brunauer–Emmett–

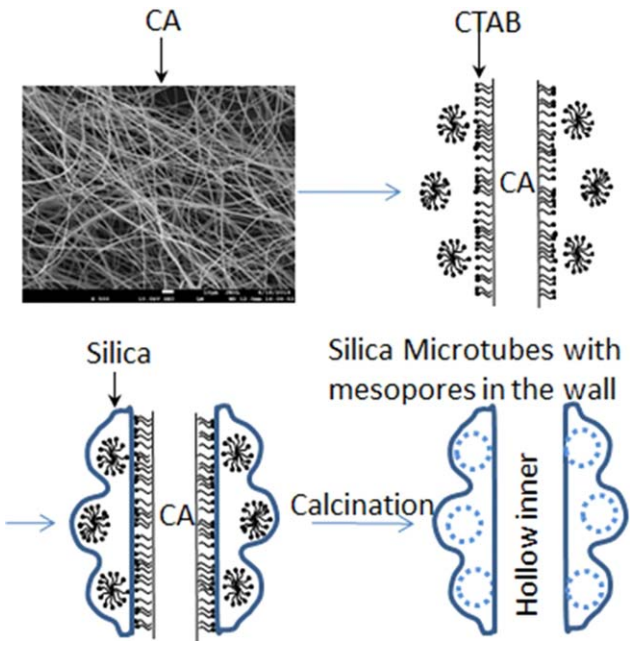

Figure 1. Schematic illustration of SMT formation. [Color figure can be viewed in the online issue, which is available at wileyonlinelibrary.com.]

Teller (BET) method. The sizes of meso and micropores were analyzed by Barrett–Joyner–Halenda and Horvath–Kawazoe models, respectively. Thermogravimetric analysis (TGA) for SMT, FSMT and FSMT-ASA was carried out using a TG209 instrument (Netzsch, German) using a heating rate of 10°C/min under a nitrogen atmosphere. An UV757 spectrophotometer (Jingke Industrial Co., Ltd. Shanghai) was used to determine the amount of ASA released from the carriers.

RESULTS AND DISCUSSION

Fabrication and Characterizations of SMT

A schematic illustration of the process used to fabricate STM is provided in Figure 1. Uniform CA electrospun fibers were used as SMTs template. The CA electrospun fibers were quite uniform, with diameters ranging from hundreds of nanometer to micrometer. Template is vital for the morphology of porous silica since it determines the inner diameter of the hollow materials. The CA electrospun fibers are relatively hydrophobic and the hydrophobic chain of CTAB is preferentially to adsorb onto the CA surface. When the surface of CA fibers is covered with CTAB, any excess CTAB will form micelles in solution. TEOS initially hydrolyzes in basic condition to form silicic acid and releases ethanol at the same time. The formed silicic acid condensates to form an oligomer and then a silica network with a large quantity of hydroxyl groups is obtained, with affinity to free and associated CTAB. Upon condensation of small silica nanoparticles, a silica shell forms on the surface of the CA fibers. Once the reaction was completed, it was very easy to separate the hybrid of silica/CA from the residue chemicals using a tweezer to pull up the whole network of hybrid and transfer to another beaker with fresh solution to clean. This is one of advantages of fabrication nanomaterials using electrospun fibers as template. The hybrid fibers were then subjected to calcination to remove the organic core and the surfactant. Condensation of adsorbed silica nanoparticles proceeds further and as a consequence robust SMTs are formed. In this process, CTAB has two principle functions. It bridges between CA fibers and TEOS sol and acts as a micro- and mesopore generator. The versatile functions of CTAB have been described elsewhere in the process of silica nanotubes fabrication through the hard-templating of cellulose nanocrystals.[18,52]

FE-SEM and TEM images of the SMT are shown in Figure 2(a,b). The hollow structure of the microtubes is apparent, as the arrows indicate in the figures. The lengths of the microtubes were between 2 and 10 μm. The original silica product obtained after calcination consisted of continuous silica microfibers that broke into micrometer-sized microtubes during sample preparation for SEM and TEM imaging. The silica wall thickness was about 100 nm and the inner SMT diameter was consistent with the diameter of CA fibers, ranging from hundreds of nanometers to microns. Figure 2(c) includes a high magnification image of silica particles on the wall of SMTs. It includes abundant mesopores randomly located in the tube walls of the prepared STM. Overall, the SEM and TEM images indicate that SMT combines an inner hollow structure with mesoporous tube walls.

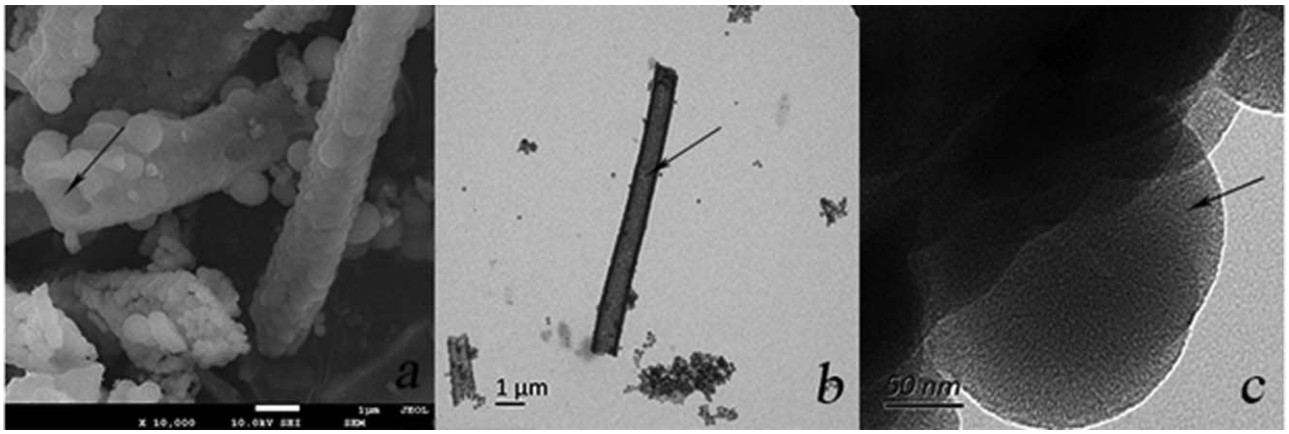

Figure 2. Field-emission scanning electron microscopy (FE-SEM) (a) and transmission (TEM) electron microscopy (b) images of SMT. A TEM image of a silica particle in the tube wall is included in (c).

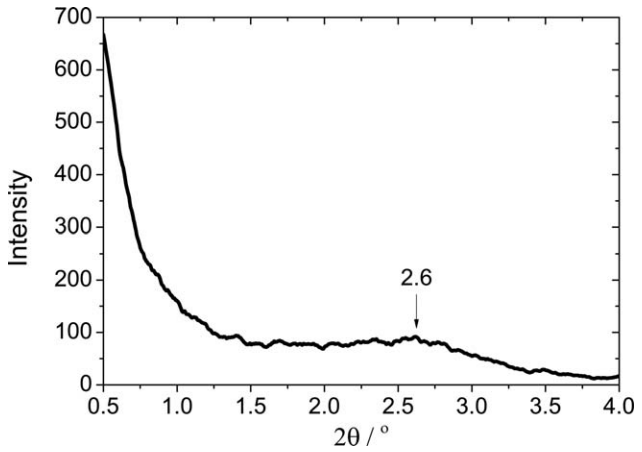

Figure 3. Small-angle X-ray diffraction (SAXD) pattern of the SMTs.

A SAXD pattern is presented in Figure 3. A very weak peak appears at about $2\theta = 2.6°$. The materials with such SAXD pattern are usually regarded as "X-ray amorphous," which are usually divided into four broad categories: disordered nanocrystalline, glassy, amorphous, and mixed.[53] The pattern indicates that the diameters of mesopores in the tube walls of SMTs are broadly distributed.

Nitrogen adsorption–desorption measurements were used to determine the specific surface areas and pore structure of the prepared SMT (Figure 4). N_2 adsorption significantly increased with the partial pressure under relative low pressures ($P/P_0 < 0.2$), ascribed to the micro- and mesopores. The samples exhibited capillary condensation from P/P_0 from 0.3 to 1. The loop observed at relative pressures (P/P_0) ranging from 0.45 to 0.85 indicates the presence of mesopores. The sharp capillary condensation that occurred at relative pressures (P/P_0) between 0.45 and 0.85 can be explained by the presence of macropores, which might originate from the inner STM hollow structure. The adsorption–desorption isotherm can be assigned to a Type IV isotherm according to IUPAC 13.2.

From the N_2 adsorption and desorption curves, pore structures and pore distribution were obtained. The BET surface area of

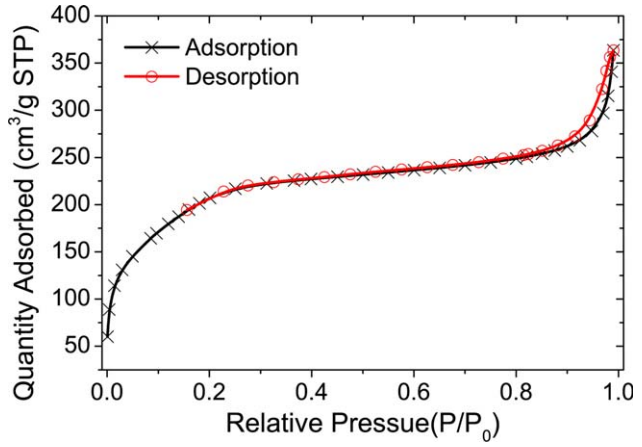

Figure 4. Nitrogen adsorption/desorption isotherms of SMTs. [Color figure can be viewed in the online issue, which is available at wileyonlinelibrary.com.]

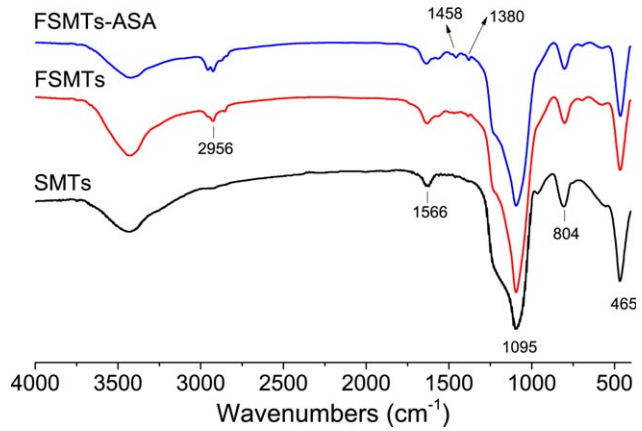

Figure 5. FTIR spectra of SMTs, FSMTs, and FSMTs-ASA. [Color figure can be viewed in the online issue, which is available at wileyonlinelibrary.com.]

the mesoporous silica nanotube was 765 m^2/g. According to the Barrett–Joyner–Halenda method, the diameter of the mesopores in the SMT walls was ~4.6 nm, and the total pore volume ~0.41 cm^3/g. The Horvath–Kawazoe pore size distribution analysis indicated a microporous median pore width of ~0.7 nm, and a maximum pore volume of ~0.18 cm^3/g. N_2 adsorption–desorption curves provided robust evidences of the existence of hierarchical structures in the SMT walls.

Amino Functionalization of SMT and Drug Delivery Profile

Untreated SMT showed poor drug delivery performance; therefore, amino silane modification was used to increase the affinity with the carboxyl group of ASA. The FTIR spectra of SMT, FSMT, and FSMT-ASA are shown in Figure 5. The FTIR spectra of SMT exhibit all the characteristic absorption peaks of silica. The peak at 1095 cm^{-1} corresponds to the antisymmetric stretching vibration of Si—O—Si. Positions of 800 and 467 cm^{-1} are assigned to the symmetric stretching vibration and the bending vibration of Si—O—Si—, respectively. Besides the characteristic absorption bands of silica, the FTIR spectra of FSMT show two pronounced peaks at 2956 and 1566 cm^{-1} that correspond to —CH_2— and N—H vibrations of grafted APTES chains, respectively. This provides evidence that amino groups

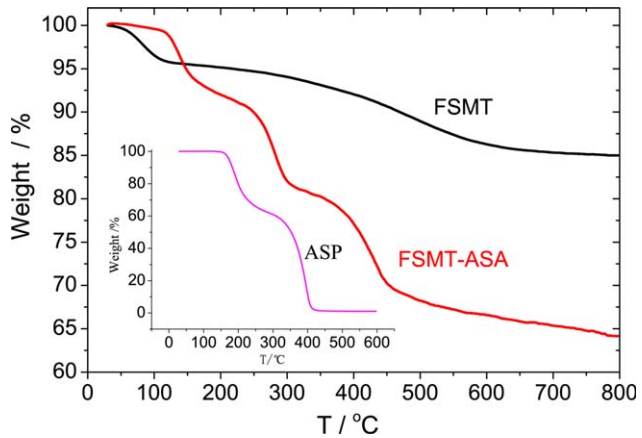

Figure 6. TGA of SMTs, FSMTs, and FSMTs-ASA. [Color figure can be viewed in the online issue, which is available at wileyonlinelibrary.com.]

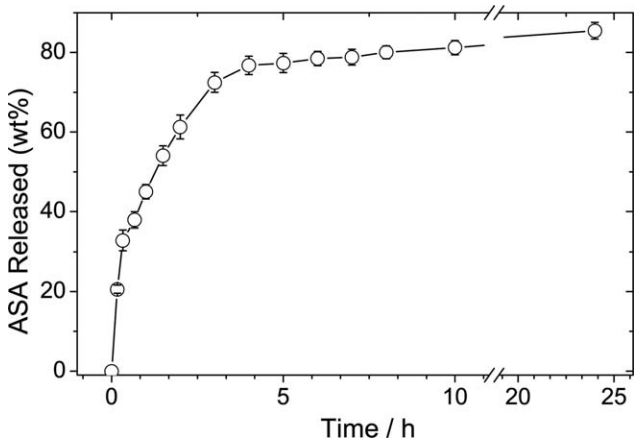

Figure 7. ASA release profile of FMSTs.

were successfully grafted on the surface of SMT. Compared with the spectra of FSMT, two relatively weaker peaks at 1450 and 1380 cm^{-1} for FSMT-ASA can be assigned to phenyl group of ASA, whereas the characteristic carbonyl peak carboxylic acid with the amino groups of ASA is present in small amounts in the sample.[48]

TGA was conducted to calculate the amount of grafted polymer and ASA loaded on the SMT surface. As shown in Figure 6, weight loss occurs between 250°C to 660°C, and an APTES loading of 9.5% (w : w) is determined according to the weight loss in the temperature range. The thermogram of pure ASA exhibits two distinct weight losses beginning at 150°C and ending at 410°C. Although the thermogram of FSMT-ASA shows three weight losses steps, one more step compared with pure ASA at 260°C. This may be caused by chemical bonding formed between amino group of FSMT and carboxyl groups of ASA. On comparison of the thermograms for FSMT and FSMT-ASA in the temperature range from 150°C to 410°C, the ASA loading was calculated to be 15% (w : w).

Figure 7 illustrates the drug release profile from FSMT-ASA in phosphate buffer solution of pH = 7.4, which can be divided in two stages with a sustained release during the first 6 h. The released amount reaches up to 79% as of total drug loading assessed by TGA. After 6 h, the release rate slows down, and the maximum release amount is determined to be 86% after 24h. This demonstrates that the functionalized STM are promising in controllable drug delivery.

The scattered points in Figure 7 could be fitted by a hyperbolic function as follows: $Qt = t/(a + bt)$. Thereto, Qt is the drug-released percentage at time t, and a and b are adjustable parameters with phenomenological meanings: $1/a$ and $1/b$ express the initial release rate (slope of the release curve at time $t = 0$) and the maximum release, respectively.[54,55] This function can be linearized to $t/Qt = a + bt$ and then regressed by the least-square method. In our case, the regressed parameters of a and b are 0.0086 and 0.0114, respectively, and with high correlation of R^2 (0.9996). Thus, the fitted function is $Qt = t/(0.0086 + 0.0114t)$. The value of $1/a$ is quite small, suggesting that the initial release rate of ASA was high. The value of $1/b$ is 88, indicating that the maximum release can reach to up 88% of total ASA loading.

There were some reports on the drug delivery of ASA by mesoporous silica nanoparticles. For example, the loading of ASA using modified MCM-41 as carrier by Vyskočilová *et al.*[56] reached up to more than 30%. However, the controlled-release time was less than 150 min. The much higher drug loading than our case can be explained by the different loading medium used. Datt *et al.*[48] studied ASA loading and release from hollow silica nanoparticles functionalized with aminopropyl groups via co-condensation or post-synthesis modification methods and determined ASA loading capacity ranging from 10% to 17% with a delivery time of less than 50 min. The ASA loading capacity of FSMT obtained in this study is very close to the higher end of their products but with a much longer releasing time. Gao *et al.*[49] synthesized two mesoporous silica nanoparticles; one was bimodal mesoporous silica nanoparticles with large pores of 24 nm and the other was small pores of 2.9 nm. Both mesoporous silica nanoparticles improved the time of ASA release to 10–14 h. However, the ASA loading capacity in this latter study with bimodal mesoporous silica nanoparticles and mesoporous silica nanoparticles was 10.3% and 5.8%, respectively. The ASA loading capacity of FSMT obtained in our experiment is higher than these systems but with a comparable releasing time. It is apparent that the cavities present in the synthesized materials are beneficial for drug loading, whereas the mesoporous structure positively affects controlled release. In our case, the hollow inner templated from CA fibers is much larger than the diameters of conventional mesoporous silica materials and hollow mesoporous silica spheres. As a consequence, our SMT displays a high drug-loading capacity. Moreover, SMT formation assisted with CTAB brings abundant micro- and mesopores on the walls of the silica tubes. Therefore, SMTs template directed with CA electrospun fibers and CTAB combine both the advantages of hollow and mesoporous materials for a high drug loading capacity and sustained release profile. The methodology of using hierarchical pores to improve both drug loading and sustained release rate was also reported by Pang *et al.*[57] In their ASA carrier system, mesoporous silica nanospheres with radially oriented mesochannels were fabricated.

CONCLUSIONS

Hierarchical SMTs with micro- and mesoporous walls were developed by using CA electrospun fibers templates, CTAB as micro- and mesopore generator, water and ethanol as the solvent, aqueous ammonia as the catalyst, and TEOS as the silica source. The prepared SMTs were uniform, with inner diameters in the submicron size and shell thicknesses of about 100 nm. BET-specific surface area of STM was 765 m^2/g. After amino postgrafting on the surface of silica tubes, the functional materials displayed a superior ASA loading capacity of up to 15% and a slow drug delivery profile with a 79% ASA controlled release in 6 h. The observed performance of the synthesized SMT is a consequence of a combination of hollow and mesoporous characteristics, which make them promising in applications for drug release and may have many potential applications in other fields.

ACKNOWLEDGMENTS

The authors are grateful for the support of Special Fund for Forestry Scientific Research in the Public Interest (201404510), National Natural Science Foundation of China (31270613), Scientific Research Foundation for the Returned Overseas Chinese Scholars, China Scholarship Council, Qing Lan Project, and the Priority Academic Program Development of Jiangsu Higher Education Institutions.

REFERENCES

1. Li, Y.; Shi, J. *Adv. Mater.* **2014**, *26*, 3176.
2. Wu, S.-H.; Mou, C.-Y.; Lin, H.-P. *Chem. Soc. Rev.* **2013**, *42*, 3862.
3. Huang, W.; Zhu, Y.; Tang, J.; Yu, X.; Wang, X.; Li, D.; Zhang, Y. *J. Mater. Chem. A* **2014**, *2*, 8839.
4. Popat, A.; Hartono, S. B.; Stahr, F.; Liu, J.; Qiao, S. Z.; Lu, G. Q. *Nanoscale* **2011**, *3*, 2801.
5. El-Toni, A. M.; Habila, M. A.; Ibrahim, M. A.; Labis, J. P.; Alothman, Z. A. *Chem. Eng. J.* **2014**, *251*, 441.
6. Sahu, S.; Sinha, N.; Bhutia, S. K.; Majhi, M.; Mohapatra, S. *J. Mater. Chem. B* **2014**, *2*, 3799.
7. Otero-Lorenzo, R.; Davila-Ibanez, A. B.; Comesana-Hermo, M.; Correa-Duarte, M. A.; Salgueirino, V. *J. Mater. Chem. B* **2014**, *2*, 2645.
8. Ma, J.; Lin, H.; Xing, R.; Li, X.; Bian, C.; Xiang, D.; Guo, W.; Qu, F. *J. Sol-Gel Sci. Technol.* **2014**, *69*, 364.
9. Buyukserin, F.; Altuntas, S.; Aslim, B. *RSC Adv.* **2014**, *4*, 23535.
10. Singh, R. K.; Kim, T.-H.; Kim, J.-J.; Lee, E.-J.; Knowles, J. C.; Kim, H.-W. *RSC Adv.* **2013**, *3*, 8692-8704.
11. Chen, F.; Hong, H.; Shi, S.; Goel, S.; Valdovinos, H. F.; Hernandez, R.; Theuer, C. P.; Barnhart, T. E.; Cai, W. *Sci. Rep.* **2014**, *4*, 5080.
12. Wang, D.; Xu, Z.; Chen, Z.; Liu, X.; Hou, C.; Zhang, X.; Zhang, H. *ACS Appl. Mater. Interfaces* **2014**, *6*, 12600.
13. Chen, X.; Klingeler, R.; Kath, M.; El Gendy, A. A.; Cendrowski, K.; Kalenczuk, R. J.; Borowiak-Palen, E. *ACS Appl. Mater. Interfaces* **2012**, *4*, 2303.
14. Yang, G.; Gai, S.; Qu, F.; Yang, P. *ACS Appl. Mater. Interfaces* **2013**, *5*, 5788.
15. Kwon, S.; Singh, R. K.; Kim, T.-H.; Patel, K. D.; Kim, J.-J.; Chrzanowski, W.; Kim, H.-W. *Acta Biomater.* **2014**, *10*, 1431.
16. Shen, J.; Song, G.; An, M.; Li, X.; Wu, N.; Ruan, K.; Hu, J.; Hu, R. *Biomaterials* **2014**, *35*, 316.
17. Ma, X.; Zhao, Y.; Ng, K. W.; Zhao, Y. *Chem. Eur. J.* **2013**, *19*, 15593.
18. Song, J. L.; Fu, G. S.; Cheng, Q.; Jin, Y. C. *Ind. Eng. Chem. Res.* **2014**, *53*, 708.
19. Song, J. L.; Wang, C. X.; Hinestroza, J. P. *Cellulose* **2013**, *20*, 1727.
20. Song, J. L.; Rojas, O. J. *Nord. Pulp Pap. Res. J.* **2013**, *28*, 216.
21. Song, J.; Birbach, N. L.; Hinestroza, J. P. *Cellulose* **2012**, *19*, 411.
22. Zhou, X.; Cheng, X.; Feng, W.; Qiu, K.; Chen, L.; Nie, W.; Yin, Z.; Mo, X.; Wang, H.; He, C. *Dalton Trans.* **2014**, *43*, 11834.
23. Zhang, Y.; Xu, Y.; Lu, Y.; Zhao, L.; Song, L. *Nanotechnology* **2013**, *24*, 315701.
24. Meng, L.; Arnoult, O.; Smith, M.; Wnek, G. E. *J. Mater. Chem.* **2012**, *22*, 19412.
25. Chen, S.; Hao, Y.; Cui, W.; Chang, J.; Zhou, Y. *J. Mater. Sci.* **2013**, *48*, 6567.
26. Liu, L.; He, D.; Wang, G.-S.; Yu, S.-H. *Langmuir* **2011**, *27*, 7199.
27. Tayi, A. S.; Pashuck, E. T.; Newcomb, C. J.; McClendon, M. T.; Stupp, S. I. *Biomacromolecules* **2014**, *15*, 1323.
28. Ras, R. H. A.; Ruotsalainen, T.; Laurikainen, K.; Linder, M. B.; Ikkala, O. *Chem. Commun.* **2007**, 1366.
29. Yu, D.-G.; White, K.; Chatterton, N.; Li, Y.; Li, L.; Wang, X. *RSC Adv.* **2015**, *5*, 9462.
30. Nagamine, S.; Tanaka, Y.; Ohshima, M. *Chem. Lett.* **2009**, *38*, 258.
31. Qiu, Y.; Yu, J. *Solid State Commun.* **2008**, *148*, 556.
32. Gao, Y.; Li, X.; Gong, J.; Fan, B.; Su, Z.; Qu, L. *J. Phys. Chem. C* **2008**, *112*, 8215.
33. Zhang, Z.; Li, X.; Wang, C.; Wei, L.; Liu, Y.; Shao, C. *J. Phys. Chem. C* **2009**, *113*, 19397.
34. Ochanda, F.; Cho, K.; Andala, D.; Keane, T. C.; Atkinson, A.; Jones, W. E., Jr. *Langmuir* **2009**, *25*, 7547.
35. Choi, S.-H.; Ankonina, G.; Youn, D.-Y.; Oh, S.-G.; Hong, J.-M.; Rothschild, A.; Kim, I.-D. *ACS Nano* **2009**, *3*, 2623.
36. Qiu, Y.; Yu, J.; Tan, C.; Yin, J.; Zhou, X. *Chem. Lett.* **2008**, *37*, 1114.
37. Zhou, J.; Gao, Q.; Fukawa, T.; Shirai, H.; Kimura, M. *Nanotechnology* **2011**, *22*, 275501.
38. Ochanda, F.; Jones, W. E., Jr. *Langmuir* **2007**, *23*, 795.
39. Nair, S.; Hsiao, E.; Kim, S. H. *Chem. Mater.* **2009**, *21*, 115.
40. Peng, Q.; Sun, X.-Y.; Spagnola, J. C.; Hyde, G. K.; Spontak, R. J.; Parsons, G. N. *Nano Lett.* **2007**, *7*, 719.
41. Huang, Z.; Chen, Y.; Zhou, W.; Nie, H.; Hu, Y. *Mater. Lett.* **2009**, *63*, 1803.
42. Yu, D.-G.; Li, X.-Y.; Wang, X.; Chian, W.; Liao, Y.-Z.; Li, Y. *Cellulose* **2013**, *20*, 379.
43. Han, S. O.; Son, W. K.; Youk, J. H.; Lee, T. S.; Park, W. H. *Mater. Lett.* **2005**, *59*, 2998.
44. Rojanarata, T.; Plianwong, S.; Su-Uta, K.; Opanasopit, P.; Ngawhirunpat, T. *Talanta* **2013**, *115*, 208.
45. Bazhenov, V. V.; Wysokowski, M.; Petrenko, I.; Stawski, D.; Sapozhnikov, P.; Born, R.; Stelling, A. L.; Kaiser, S.; Jesionowski, T. *Int. J. Biol. Macromol.* **2015**, *76*, 33.
46. Ehrlich, H.; Simon, P.; Motylenko, M.; Wysokowski, M.; Bazhenov, V. V.; Galli, R.; Stelling, A. L.; Stawski, D.; Ilan, M.; Stoecker, H.; Abendroth, B.; Born, R.; Jesionowski, T.; Kurzydlowskii, K. J.; Meyer, D. C. *J. Mater. Chem. B* **2013**, *1*, 5092.
47. Huang, J.; Gu, Y. *Curr. Opin. Colloid Interface Sci.* **2011**, *16*, 470.

48. Datt, A.; El-Maazawi, I.; Larsen, S. C. *J. Phys. Chem. C* **2012**, *116*, 18358.

49. Gao, L.; Sun, J.; Li, Y. *J. Solid State Chem.* **2011**, *184*, 1909.

50. Klapiszewski, L.; Bartczak, P.; Wysokowski, M.; Jankowska, M.; Kabat, K.; Jesionowski, T. *Chem. Eng. J.* **2015**, *260*, 684.

51. Han, W. S.; Kang, Y.; Lee, S. J.; Lee, H.; Do, Y.; Lee, Y. A.; Jung, J. H. *J. Phys. Chem. B* **2005**, *109*, 20661.

52. Fu, G.; He, A.; Jin, Y.; Cheng, Q.; Song, J. *Bioresources* **2012**, *7*, 2319.

53. Zhang, Y.; Liu, X.; Huang, J. *ACS Appl. Mater. Interfaces* **2011**, *3*, 3272.

54. He, Q.; Shi, J.; Chen, F.; Zhu, M.; Zhang, L. *Biomaterials* **2010**, *31*, 3335.

55. Arcos, D.; Lopez-Noriega, A.; Ruiz-Hernandez, E.; Terasaki, O.; Vallet-Regi, M. *Chem. Mater.* **2009**, *21*, 1000.

56. Vyskočilová, E.; Lusticka, I.; Paterova, I.; Machova, L.; Cerveny, L. *Solid State Sci.* **2014**, *38*, 85.

57. Pang, J.; Li, X.; Zhou, G.; Sun, B.; Wei, Y. *RSC Adv.* **2015**, *5*, 6599.